

Structure-Dependent All-Optical Switching in Graphene-Nanoribbon-Like Molecules: Fully Conjugated Tri(perylene bisimides)

Huan Wang,^{†,§} Hongmei Su,^{*,†,§} Hualei Qian,^{‡,§} Zhaohui Wang,^{*,‡,§} Xuefei Wang,^{†,§} and Andong Xia^{*,†,§}

The State Key Laboratory of Molecular Reaction Dynamics, Institute of Chemistry, Chinese Academy of Sciences, Beijing 100190, People's Republic of China, The CAS Key Laboratory of Organic Solids, Institute of Chemistry, Chinese Academy of Sciences, Beijing 100190, People's Republic of China, and Beijing National Laboratory for Molecular Sciences (BNLMS), Institute of Chemistry, Chinese Academy of Sciences, Beijing 100190, People's Republic of China

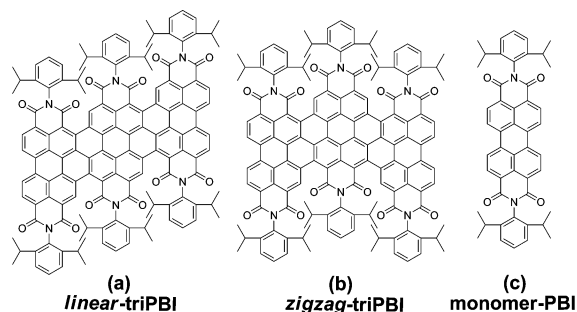
Received: June 18, 2010; Revised Manuscript Received: July 20, 2010

We present the structure-dependent nonlinear optical (NLO) properties of fully conjugated tri(perylene bisimides) (triPBIs) toward the understanding of the role of conformational flexibility and π -electron conjugation in molecular NLO properties of model graphene-nanoribbon (GNR)-like molecules. In the present paper, we report the NLO absorption properties of the triPBIs in toluene excited at 532 nm with nanosecond laser pulses, where the observed transient excited state is determined to be a triplet and presented in the nonlinear process similar to the NLO properties that occur in C₆₀. As a result, the all-optical switching in both visible and near-infrared regions upon excitation at 532 nm was demonstrated, suggesting that the chemically synthesized model GNRs act well as smart all-optical switching devices without the need of external control. Furthermore, Raman spectral measurement was further used to characterize the conjugated structure properties of model compounds of functionalized graphene nanoribbons (F-GNRs), while the dispersion and splitting of the G-band and D-band in both frequency and intensity can help to distinguish the π -conjugation and conformational flexibility of the two different triPBI isomers, showing the opportunity to tailor their optoelectronic properties by precisely controlling the edge orientation, edge width, and chemical termination of the edges in the synthesized F-GNRs.

Introduction

Graphene is a one-atom-thick planar sheet of sp²-bonded carbon atoms, which exhibit novel electronic properties, such as high carrier mobility,^{1,2} ballistic transport,^{3,4} massless Dirac fermions,^{5–8} quantum Hall effect,^{9–12} and localization suppression.¹³ Recently, a few reports have focused on the optical limiting properties of graphene families, including graphene oxide nanosheets, graphene nanosheets, graphene oxide nanoribbons, and graphene nanoribbons, where the observed nonlinear optical (NLO) responses were reported to be mainly induced by the nonlinear scattering mechanism.^{14–16} Because of the absence of a band gap, most of the studies of optical and optoelectronic properties of graphene have remained theoretical.^{4,17–22} Thus, particular attention has been paid to prepare graphene into a narrow graphene nanoribbon (GNR), where the opening of an energy gap in determining GNR optical properties was expected because of the confinement and edge effects.^{18,23} This makes GNR a very promising candidate material for applications in carbon-based photonic and optoelectronic. Driven by these, many methods, such as lithography,²⁴ exfoliation of graphite or heat treatment of silicon carbide,^{25,26} chemical approaches,^{23,27,28} and self-assembly processes,^{29,30} have been devoted for preparation of GNRs. Among them, particular organic synthetic protocols have been found to easily produce

SCHEME 1: Molecular Structures of Two Structural Isomers of triPBIs^a



^a The linear-triPBI (a) and zigzag-triPBI (b). The structure of monomer PBI (c) is also shown for comparison.

functionalized graphene nanoribbon (F-GNR) structures with the desired shape and dimensions required for fundamental and practical applications.^{27,28} Although the optoelectronic properties of these organic synthetic nanoribbons have yet to be characterized, they may indeed exhibit graphene-like behavior.

Due to lack of well-prepared GNR samples, very few works concerning the opened energy gap in GNRs have been experimentally explored until now.^{23,31} In our previous research, we presented the successful synthesis of fully conjugated tri(perylene bisimides) (triPBIs), having 19 six-membered carbon rings in the core and 6 imide groups at the edges, providing an ideal model compound for a systematic study of the structure–property relationships of F-GNRs.²⁷ Scheme 1 shows the molecular structures of two structural isomers of

* To whom correspondence should be addressed. E-mail: hongmei@iccas.ac.cn (H.S.); wangzhaohui@iccas.ac.cn (Z.W.); andong@iccas.ac.cn (A.X.).

[†] The State Key Laboratory of Molecular Reaction Dynamics.

[‡] The CAS Key Laboratory of Organic Solids.

[§] Beijing National Laboratory for Molecular Sciences (BNLMS).

triPBIs (linear-triPBI and zigzag-triPBI). The electrochemical properties of the two triPBI structural isomers have been reported.²⁷ The properties of the two triPBIs suggest that their high electron affinities make them suitable for application as n-type functional components in optoelectronic devices. In the present study, we report the NLO absorption properties of the triPBIs in toluene excited at 532 nm with nanosecond laser pulses, where the observed transient excited state is determined to be a triplet and plays important roles in the nonlinear process, similar to C₆₀. This work shows that the chemically synthesized F-GNRs act well as smart all-optical switching devices without the need for external control. Furthermore, the different structural properties of the model F-GNRs concerning the symmetry breaking have also been characterized by Raman spectroscopy. The pronounced Raman G-band and D-band splitting and dispersion are investigated to correlate the different behaviors observed in the linear and NLO properties with the topology of the π -electron system of triPBIs.

Materials and Methods

1. Materials. Fully conjugated tri(perylene bisimides) linear-triPBI and zigzag-triPBI were synthesized as described elsewhere.²⁷ The lengths/widths of linear-triPBI and zigzag-triPBI were estimated to be about 1.879 nm/0.864 nm and 1.870 nm/0.864 nm, respectively, after structural optimization with the Gaussian03 package at the B3LYP/3-21G level.³² C₆₀ powder was purchased from Aldrich without further purification. The toluene used in this study was HPLC grade.

2. General Methods. Steady-State Spectroscopy. Absorption spectra were recorded with a UV–vis spectrophotometer (Model U-3010, Hitachi). Fluorescence spectra were measured with a fluorescence spectrophotometer (F4600, Hitachi).

Laser Flash Photolysis. Nanosecond time-resolved transient absorption spectra were measured using a nanosecond flash photolysis setup Edinburgh LP920 spectrometer (Edinburgh Instruments Ltd.), combined with a Nd:YAG laser (Surelite II, Continuum Inc.). The sample was excited by a 532 nm laser pulse (1 Hz, fwhm \approx 7 ns). The analyzing light was from a 450 W pulsed xenon lamp. A monochromator equipped with a photomultiplier for collecting the spectral range from 350 to 850 nm and an InGaAs detector for collecting the spectral range from 900 to 1600 nm was used to analyze transient absorption spectra. Samples were freshly prepared for each measurement and were adjusted to an absorbance of about 0.25 in 10 mm path length quartz cuvettes at the laser wavelength used. Data were analyzed by the online software of the LP920 spectrophotometer. The fitting quality was judged by weighted residuals and a reduced χ^2 value.

Nonlinear Transmission and Optical Bistability Measurement. The standard setup for optical limiting measurements was used as described in ref 33. All of the samples were dissolved in toluene with the transmission $T \approx 60\%$ at 532 nm in 10 mm path length quartz cuvettes. The second harmonic at 532 nm, from a nanosecond Nd:YAG pulsed laser (Surelite II, Continuum Inc., fwhm \approx 7 ns), was used as the laser source. The laser beam was well-aligned by an inverted telescope system and then filtered by an aperture to obtain a nearly homogeneous light spot. Before entering the sample, the laser beam was divided into two beams (\sim 1:5) by a beamsplitter, where the reflected beam was used as the reference and the transmitted one was focused onto the sample by a 15 cm focal length lens. The sample was placed about 2 cm in front of the focus, where the spot diameter was about 0.7 mm. The incident laser intensity was changed by rotating a half-wave plate placed before the

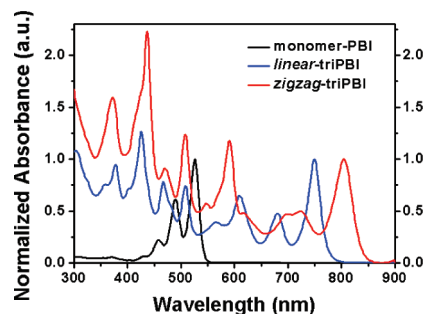


Figure 1. Normalized UV–vis spectra of linear-triPBI and zigzag-triPBI. The absorption spectrum of monomer PBI is also shown for comparison. The intensities of these samples are normalized to the peak of linear-triPBI at 749 nm.

Glan–Thomson polarizer, and the incident and transmitted laser powers were monitored by two separated energy detectors.

The experimental setup for optical bistability measurements was similar to the main part of the optical limiting, except for the detectors. To detect the time profile transformations of a single laser pulse before and after the samples, fast response photodiodes (DET210, Thorlabs) were used, which have a fast rise time of less than 1 ns. The signal outputs from photodiodes were then input into a digital storage oscilloscope (Tektronix, TDS 3052B, 500 MHz). The synchronous output signals from the Nd:YAG laser were used to trigger the oscilloscope in order to make sure of the simultaneity of the rising time of the input and output profiles.

To avoid thermal effects, single-pulse shots were used, and all of the transmitted beams were collected by the power meter. The experiments were repeated several times with the same set of samples, and consistent results were obtained, demonstrating the good photochemical stability of the samples at these experimental conditions.

Raman Spectroscopy. Raman spectral measurements were performed at room temperature with a JY HR-800 confocal Raman microscopy system equipped with a 457 nm laser. To avoid sample damage or laser-induced heating, the incident laser power was controlled to about 1 mW. The Si peak at 520 cm⁻¹ was used as a reference for wavenumber calibration.

Results and Discussion

Figure 1 shows the UV–vis absorption spectra of linear-triPBI and zigzag-triPBI in toluene. For comparison, the absorption of monomer PBI is also shown in Figure 1. It is found that both linear-triPBI and zigzag-triPBI show broad redshifted absorption bands which cover almost the entire visible region compared with that of monomer PBI. The major absorption bands of linear-triPBI and zigzag-triPBI are located at 378, 427, 466, 508, 609, 680, and 749 nm and 373, 437, 508, 590, 696, and 804 nm, respectively. The abundant absorption bands result from largely extensive conjugation over the π -electronic system of these triPBIs. The UV–vis spectrum of zigzag-triPBI is bathochromically shifted by about 55 nm with respect to that of linear-triPBI, suggesting a more efficient conjugation in zigzag-triPBI as compared to that in linear-triPBI.

Similar to the monomer PBI, the fluorescence spectra of the model F-GNRs (see Figure S2 in Supporting Information) display nearly a mirror symmetry relationship to the visible portions of their absorption spectra, but the fluorescence is very weak, with quantum yields of about 2.86×10^{-2} (zigzag-triPBI) and 5.59×10^{-2} (linear-triPBI), and the fluorescence lifetimes are about 0.23 (zigzag-triPBI) and 2.4 ns (linear-triPBI), respectively.

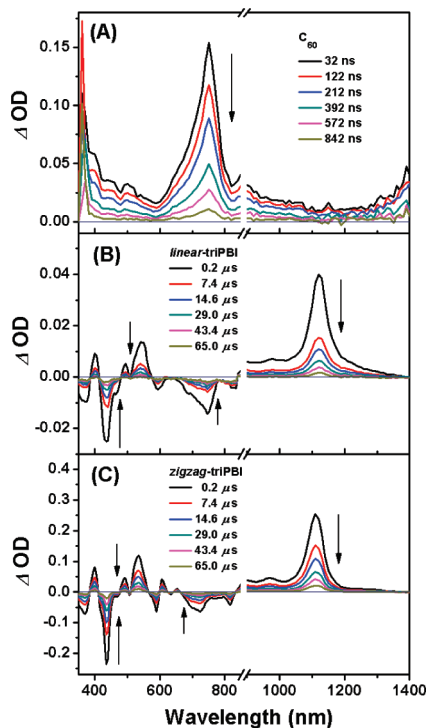


Figure 2. Transient absorption spectra of (A) C_{60} , (B) linear-triPBI, and (C) zigzag-triPBI at different delay times after a pulsed excitation at 532 nm.

Figure 2 shows the nanosecond transient absorption spectra of the linear-triPBI and zigzag-triPBI solutions in toluene after laser flash photolysis at 532 nm. There are two main triplet excited-state absorptions located at the wavelengths around 535 and 1110 nm. The recorded transient signals at different wavelengths in a time resolution of less than 10 ns are shown in Figures S3–S5 (see Supporting Information). A fitting of all of the data can be obtained with a biexponential decay. It must be mentioned here that, in our previous works,²⁷ we found that for both linear-triPBI and zigzag-triPBI, the difference in ground-state absorption spectra (and molecular orbital energies) between the helical and nonhelical structures was almost negligible. From the fitted results at different peak wavelengths as listed in Table S1 (see Supporting Information), it is found that all of the transient signals also show almost the identical decay dynamics with two distinct time constants (fractions) around $0.72 \mu\text{s}$ (82.8%) and 17 (17.2%) for linear-triPBI and around 4.5 (48%) and $30 \mu\text{s}$ (52%) for zigzag-triPBI at different wavelengths. The two different time constants obtained mainly correspond to their two stable helical and nonhelical configurations for each triPBI isomer, respectively.²⁷ The preexponential factors may represent the fractions of the stable helical and nonhelical configurations in each triPBI isomer. All of the observed excited-state absorptions result from their lowest triplet state since all of them have similar decay dynamics in each triPBI (see Table S1 in Supporting Information). To prove this point or to see if one of the two components in each triPBI is from radicals or charge-transfer states, ethyl iodide is added to the zigzag-triPBI solution as a control for laser photolysis measurements (see Figure S5 and Table S2 in Supporting Information). For ethyl iodide, because of the heavy-atom effect, it is expected that the intersystem crossing could become more significant and lead to the increase of triplet-state yield.^{34,35} As a result, we observe the increased intensities of all of the excited-state absorption peaks after adding ethyl iodide. Furthermore, the preexponential factors of two distinct components remain

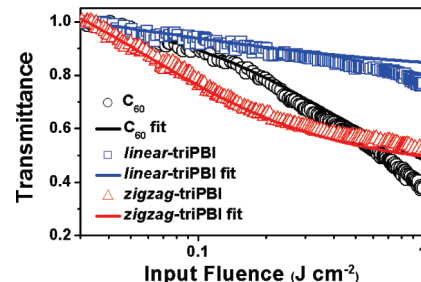


Figure 3. Plots of normalized optical transmission against the incident laser pulse energy with $T = 60\%$ at 532 nm; C_{60} (open circle), linear-triPBI (open square), zigzag-triPBI (open triangle). Solid lines are the fitting results based on the five-level model.

unchanged before and after adding ethyl iodide, indicating that all of the excited-state absorptions are from the triplet; otherwise, the ratio of the preexponential factors could be changed if one of them is from radicals or charge-transfer states. Obviously, the zigzag-triPBI shows stronger excited-state absorptions relative to linear-triPBI, as shown in Figure 2, when both of them have the same ground-state absorbance (0.25) at 532 nm during transient absorption measurements, suggesting that a stronger NLO response occurred in zigzag-triPBI.

For the nonlinear transmission measurements, the concentrations of all of the samples were adjusted so that the low-fluence linear transmissions at 532 nm through the cuvette were the same at about 60%. Figure 3 shows the nonlinear transmission curves of linear-triPBI and zigzag-triPBI in toluene at 532 nm. For comparison, the result of C_{60} in toluene solution recorded under the same conditions is also included in Figure 3. Experiments with toluene alone afforded no detectable transmission change, indicating that the solvent contributions are negligible. It is found that zigzag-triPBI exhibits an optical limiting performance with a rapid decrease in transmittance at fluences of lower than 0.5 J cm^{-2} , which is much better than that of the C_{60} solution. Although the optical limiting threshold value (the limiting threshold fluence, F_{lim} , defined as the fluence at which the transmittance is half of the linear one³⁶) of zigzag-triPBI is at the same level as that of C_{60} , which is around 0.5 J cm^{-2} at the same experimental conditions, the observed optical limiting properties of zigzag-triPBI under nanosecond pulsed excitation are stronger than that of C_{60} and seldom found in other molecule systems. The optical limiting performance of the excited-state absorptions can be characterized by the ratio of the excited-state to ground-state absorption cross sections, σ_T/σ_G , where the larger the σ_T/σ_G , the better the optical limiting performance. Referring to the reverse saturable absorption (RSA) that occurred in C_{60} ,^{37–39} obviously, the excited states of zigzag-triPBI involved in the NLO effect possess much larger excited-state absorption cross sections, σ_T , with respect to the ground state at 532 nm. Conversely, the linear transmittance of linear-triPBI shows a slight decrease as the incident fluences increase because of the much weaker excited-state absorption relative to zigzag-triPBI, as shown in Figures 2 and 3.

The distinct differences in the nonlinear transmission effects between linear-triPBI and zigzag-triPBI mainly result from their different excited-state absorption upon excitation with nanosecond laser pulses. To test the RSA hypothesis in linear-triPBI and zigzag-triPBI, a five-level model was used to fit the observed nonlinear transmission for C_{60} , linear-triPBI, and zigzag-triPBI (see Supporting Information).⁴⁰ Stimulated emission from the first excited state to the ground state was not included, owing to the very low fluorescence quantum yields of C_{60} , linear-triPBI, and zigzag-triPBI.

TABLE 1: Fitted Results of Nonlinear Optical (NLO) Responses at 532 nm (7 ns) Based on the Five-Level Model for C₆₀, linear-triPBI, and zigzag-triPBI

samples	C ₆₀			linear-triPBI			zigzag-triPBI		
	0.2	0.5	OL ^b	(OB) ^a	(OB) ^a	OL ^b	(OB) ^a	(OB) ^a	OL ^b
fluence (J cm ⁻²)	(OB) ^a	(OB) ^a	OL ^b	(OB) ^a	(OB) ^a	OL ^b	(OB) ^a	(OB) ^a	OL ^b
c(×10 ⁻⁵) (M)		42.04			1.74			1.04	
τ _S (ns)		1.2			2.4			0.23	
τ _T (ns)		322			4057			17910	
τ _{ISC} (ns)	1.32	1.24	1.75	2.74	3.17	2.57	2.89	2.42	2.21
σ _G (×10 ⁻¹⁸) (cm ²)		1.97			46.5			78.8	65.6
σ _S (×10 ⁻¹⁸) (cm ²)	11.7	9.76	12	16.5	14.4	16.5	154	126	133
σ _T (×10 ⁻¹⁸) (cm ²)	6.34	6.3	5.42	83.7	88.4	79.4	268	252	248
σ _T /σ _G	3.22	3.2	2.75	1.8	1.9	1.71	3.4	3.2	3.78
hysteresis loop area (rel.)	0.20	0.29		0.19	0.14		0.26	0.21	

^a OB represents the optical bistable measurement. ^b OL represents the optical limiting measurement.

On the basis of the five-level model, we obtained the best fitting results of the nonlinear transmission responses of C₆₀, linear-triPBI, and zigzag-triPBI in toluene solutions at 532 nm, as shown in Figure 3. The slight derivation from the fitting seems to have an additional component obtained from nonlinear scattering at high fluence.⁴¹ The deduced values of σ_G, σ_T, and σ_T/σ_G are listed in Table 1. The values of τ_S and τ_T for the fittings are obtained by referring to the fluorescence lifetime and transient absorption measurements (see Table S3 in Supporting Information). It is found that the σ_T/σ_G of C₆₀ of about 3.0 ± 0.3 is in agreement with previous results,³⁹ indicating the reliability of our experiments and fitting methods. We thus determined that the σ_T/σ_G of zigzag-triPBI of about 3.5 ± 0.2 is truly larger than that of linear-triPBI, which is about 1.8 ± 0.1, as mentioned above. Obviously, the observed nonlinear absorptions of the triPBIs are mainly induced by RSA, where the absorption of the triplet excited state plays the dominant role since the laser pulse width (7 ns) is larger than the intersystem cross times (around 2 ns) and fluorescence lifetimes.

For graphene, a major issue is to develop the graphene-based logic devices, while several electronic transistor behaviors from nanoribbons due to quantum confinement have been reported.^{42–44} In analogy with an electronic transistor, an all-optical device is more important in optical science and engineering, where an all-optical switch is a device in which one light beam can control another. The large σ_T/σ_G of model F-GNRs reported here will cause a light-induced increasing absorption when incident light fluence increases; thus, an all-optical bistable loop must be expected.⁴⁵

Figure 4 shows the typical all-optical bistable loops of C₆₀, linear-triPBI, and zigzag-triPBI at different incident intensities. For comparison, the bistable input–output correspondence was fitted by referring to the fitted optical limiting parameters (see Table 1) and is shown as solid curves in Figure 4. It is found that both the experimental and calculated results are in good agreement with each other. The larger hysteresis loop area suggests that the bistable performance of zigzag-triPBI is better than that of C₆₀ below the limiting threshold fluence F_{lim} (less than 0.5 J cm⁻²) because of the larger excited-state absorption cross section relative to C₆₀. The hysteresis loops are nonsquare, making the actual switching transitions diffuse. The clockwise hysteresis loop is typical of the RSA effect for mirrorless absorptive optical bistability, which can be attributed to differential absorption at the two different states (ground state and triplet state in our case), so that the local absorption is a function of position along the optical path. The hysteresis loop area, which is an important characteristic parameter for the optical bistability, can be easily controlled by the input fluences, as

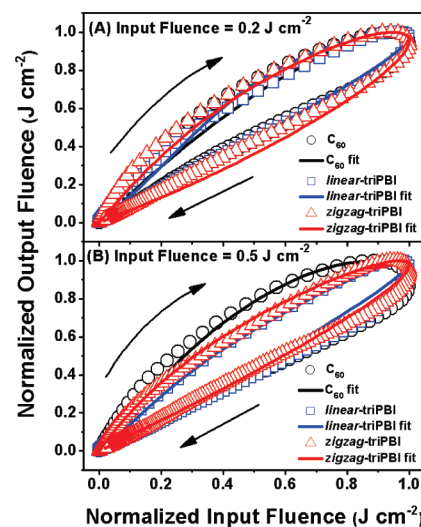


Figure 4. Optical bistable loops of linear-triPBI, zigzag-triPBI, and C₆₀ in toluene solution ($T = 60\%$) with a 532 nm, 7 ns laser pulse width. The input laser fluences are 0.2 (A) and 0.5 J cm⁻² (B). Solid lines represent the calculated curves of bistable loops corresponding to the experimental curves (up-triangles, squares, and circles).

shown in Table 1 and Figure 4. The bistable performance of C₆₀ is better than that of zigzag-triPBI above the limiting threshold fluence but only when it is working at higher laser power. Obviously, the optical switching of zigzag-triPBI has the advantages of relatively low energy with fast response time and no cavity or external feedback.

Importantly, as mentioned above, besides the optical switching that occurred at 532 nm, the transient absorption measurements also show a broad and strong excited-state absorption in the NIR region at around 1110 nm for linear-triPBI and zigzag-triPBI, which is in the optical fiber communication window (0.8–1.7 μm). It is known that development of photonic devices requires the control of the frequency and/or intensity of light in a predictable manner. If integrated with modern fiber optic technologies, optical switching in the NIR region may have important applications for optical communication and computation in telecommunication networks.

Exposure of the triPBIs to the pump beam (532 nm) causes the depopulation of the ground state and an increase in the population of the triplet states. The transmission intensity of the probe beam decreased because of the strong triplet–triplet absorption at around 1110 nm. The typical traces of the optical switching based on the triplet–triplet absorption at around 1110 nm for linear-triPBI and zigzag-triPBI are shown in Figure 5. Clearly, from the pump–probe experiments, the transmission

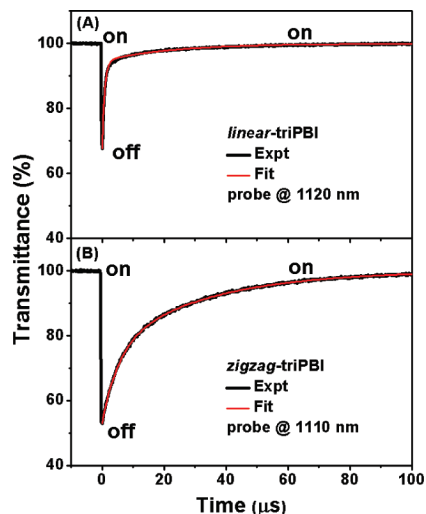


Figure 5. All-optical switching of linear-triPBI (a) and zigzag-triPBI (b) in toluene solution with the transmittance change of the probe beam (T/T_0) when pumped with a 7 ns pulse at 532 nm. T and T_0 are the transmission intensities of the probe beam with and without a pump beam. The incident energy is about 5 mJ pulse⁻¹ with a spot diameter about 4 mm in the samples. The concentrations of the samples were adjusted with the absorbance at about 0.25 at 532 nm.

(T/T_0) of the probe beam decreases with the pump beam at 532 nm on. The switching times from the on state to the off state for both linear-triPBI and zigzag-triPBI are less than 7 ns, limited by the time resolution of our experiments, and the switching times from the off state to the on state are about 19 μ s for zigzag-triPBI and about 4.4 μ s for linear-triPBI, just the same as that at 532 nm, indicating that the NLO responses at different wavelengths of triPBIs result from the same lowest triplet states. The most important experimental result is the large difference between the relative amplitudes of the transient signals, which depends mainly on the pumping intensity and sample concentrations. In our case, we achieve a relative change of the probe beam $\Delta T/T_0$ ($= (T_0 - T)/T_0$) of zigzag-triPBI of more than 47% at 1110 nm, which is much larger than that ($\sim 29\%$) at 532 nm. Conversely, because of the small σ_T/σ_G of linear-triPBI, the change of the probe beam $\Delta T/T_0$ of linear-triPBI is only obtained at about 32.3% at 1120 nm and about 13% at 532 nm. Therefore, the large change of the probe beam $\Delta T/T_0$ of zigzag-triPBI will provide the basis for the use of this type of materials to develop a high-quality optical switching in the optical fiber communication window.

Furthermore, from the structural viewpoint of F-GNRs, the observed broad and abundant absorption bands in triPBIs may also come from the confinement and broken molecule symmetry, as discussed in the literature.^{20,23,46–48} To correlate the different behavior observed in the NLO properties with the different structures of linear-triPBI and zigzag-triPBI, we performed Raman spectral measurements. Figure 6 shows the typical Raman spectra of linear-triPBI and zigzag-triPBI. Two main features are presented in the first-order Raman spectra, the G-band and the D-band, where the splittings of G-band at around 1580 cm^{-1} and the D-band at around 1350 cm^{-1} in triPBIs are clearly seen. It is known that the G-band corresponds to a Raman-active vibrational mode of graphene, and the D-band is related to defects or edges, leading to disorder and confinement.^{47,49,50} The dispersion of the G-band and D-band can distinguish the π -conjugation and conformational flexibility of graphene. As shown in Figure 6, both linear-triPBI and zigzag-triPBI have a similar frequency and intensity dispersion of the D-band but

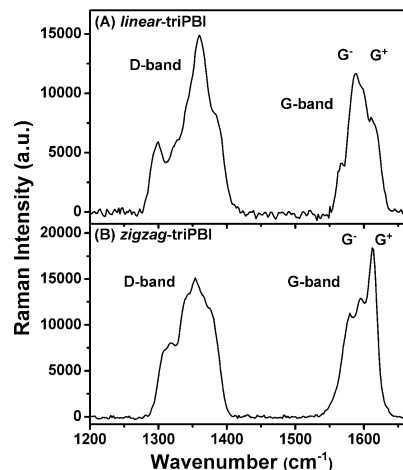


Figure 6. Raman spectra of (A) linear-triPBI and (B) zigzag-triPBI excited by a 457 nm laser. Both the D-band at $\sim 1350 \text{ cm}^{-1}$ and the G-band at $\sim 1580 \text{ cm}^{-1}$ show distinct splittings.

different G-band properties (also see the deconvolution results in Figure S7 and Table S4 in Supporting Information). The similar D-band properties indicate that the same edge or disorder effects occur in both linear-triPBI and zigzag-triPBI. The G-band splits into two (G^+ , G^-) or more bands with the phonon softening (red shifts) because of the symmetry breaking,⁵¹ where the I_{G^-}/I_{G^+} of linear-triPBI is larger than that of zigzag-triPBI, indicating that a stronger symmetry breaking occurred in linear-triPBI with a shorter delocalization length relative to that of zigzag-triPBI.^{51–54} Furthermore, by carefully checking the ratio of the intensities of the D-band (I_D) and G-band (I_G), it is found that the ratio of I_D/I_G of linear-triPBI is also larger than that of zigzag-triPBI, suggesting a reduced π -conjugation in linear-triPBI relative to that in zigzag-triPBI since the Raman D-band at around 1350 cm^{-1} is an indicator of intrinsic defects or disorder that disrupts the π -conjugation. Obviously, the observed greater NLO effects of zigzag-triPBI than those of linear-triPBI are associated with the presence of a longer delocalization length, which is manifested from the Raman band splittings that resulted from symmetry breaking.^{23,47,55}

Our previous quantum chemical calculation results indicated that three unoccupied orbitals with the same parentage in linear-triPBI and zigzag-triPBI²⁷ imply their stronger electron affinity and their ability to accept up to six electrons, which sustain the electron-acceptor properties of F-GNRs. Indeed, the theory for ideal GNRs predicts that E_{gap} depends sensitively on the boundary conditions at the edges,^{4,17,18,56} where the Raman band splittings that resulted from symmetry breaking are directly correlated to the molecular electronic structures.^{4,47,55} Since zigzag-triPBI is more conjugated than linear-triPBI, it is obvious that zigzag-triPBI has a lower band gap (E_{gap}) than linear-triPBI, as shown in Figure 1. Because of the abundant absorption bands within the visible to near-infrared region in both the singlet and triplet states of the triPBIs, wide band tunability may be obtained using the model F-GNR-like molecules as potential candidates for mirrorless all-optical switching. This has the NLO applications as expected from F-GNRs. Obviously, as mentioned above, RSA dominates the observed NLO response and optical switching behaviors of linear-triPBI, zigzag-triPBI, and C_{60} . Zigzag-triPBI exhibits a greater NLO effect than did linear-triPBI and C_{60} , which is associated with the presence of a longer delocalization length with a lower band gap and larger σ_T/σ_G in zigzag-triPBI. Further, it is important to promote the population of the triplet state for the large and fast modulation

of the probe beam $\Delta T/T_0$ with low pump intensity, where a monobay-functionalized model F-GNRs with heavy atoms (such as Cl, I and Br) in the bay regions of multi-PBIs have been successfully synthesized and are being studied in our laboratory.⁵⁷

Conclusions

In summary, we present the first experimental investigation of fast optical switching in two graphene nanoribbon-like molecules in the visible and NIR regions, which have the advantages of relatively fast response and mirrorless structure. The RSA dominates the observed NLO response, which is associated with the presence of a long delocalization length with a low band gap and a large σ_7/σ_G . Raman spectroscopy further suggests the graphene-like behavior of chemically synthesized triPBIs. The chemical synthesis strategy to the high-quality single-layer model F-GNRs opens up an exciting possibility to tailor optoelectronic structures by precisely controlling the edge orientation, edge width, and chemical termination of the edges in model F-GNRs toward the expected optoelectronic effects.

Acknowledgment. This work was supported by NSFC, 973 Program, and the Chinese Academy of Sciences.

Supporting Information Available: Steady-state spectroscopy, nanosecond time-resolved transient absorption, table of fitted parameters of time evolutions of the transient absorption at different probe wavelengths, table of parameters of triPBIs obtained from the steady-state spectrum and transient absorption measurements, five-level model and fitting details of optical limiting and optical bistability, deconvolution results of the Raman D-band and G-band of triPBIs, and complete ref 32. This material is available free of charge via the Internet at <http://pubs.acs.org>.

References and Notes

- (1) Novoselov, K. S.; Geim, A. K.; Morozov, S. V.; Jiang, D.; Zhang, Y.; Dubonos, S. V.; Grigorieva, I. V.; Firsov, A. A. *Science* **2004**, *306*, 666.
- (2) Wang, S. A.; Ang, P. K.; Wang, Z. Q.; Tang, A. L. L.; Thong, J. T. L.; Loh, K. P. *Nano Lett.* **2010**, *10*, 92.
- (3) Du, X.; Skachko, I.; Barker, A.; Andrei, E. Y. *Nat. Nanotechnol.* **2008**, *3*, 491.
- (4) Areshkin, D. A.; Gunlycke, D.; White, C. T. *Nano Lett.* **2007**, *7*, 204.
- (5) Novoselov, K. S.; Geim, A. K.; Morozov, S. V.; Jiang, D.; Katsnelson, M. I.; Grigorieva, I. V.; Dubonos, S. V.; Firsov, A. A. *Nature* **2005**, *438*, 197.
- (6) Nomura, K.; MacDonald, A. H. *Phys. Rev. Lett.* **2007**, *98*, 076602.
- (7) Park, C. H.; Yang, L.; Son, Y. W.; Cohen, M. L.; Louie, S. G. *Nat. Phys.* **2008**, *4*, 213.
- (8) Plochocka, P.; Faugeras, C.; Orlita, M.; Sadowski, M. L.; Martinez, G.; Potemski, M.; Goerbig, M. O.; Fuchs, J. N.; Berger, C.; de Heer, W. A. *Phys. Rev. Lett.* **2008**, *100*, 087401.
- (9) Zhang, Y. B.; Tan, Y. W.; Stormer, H. L.; Kim, P. *Nature* **2005**, *438*, 201.
- (10) Novoselov, K. S.; McCann, E.; Morozov, S. V.; Fal'ko, V. I.; Katsnelson, M. I.; Zeitler, U.; Jiang, D.; Schedin, F.; Geim, A. K. *Nat. Phys.* **2006**, *2*, 177.
- (11) Bolotin, K. I.; Ghahari, F.; Shulman, M. D.; Stormer, H. L.; Kim, P. *Nature* **2009**, *462*, 196.
- (12) Du, X.; Skachko, I.; Duerr, F.; Luican, A.; Andrei, E. Y. *Nature* **2009**, *462*, 192.
- (13) Morozov, S. V.; Novoselov, K. S.; Katsnelson, M. I.; Schedin, F.; Ponomarenko, L. A.; Jiang, D.; Geim, A. K. *Phys. Rev. Lett.* **2006**, *97*, 016801.
- (14) Wang, J.; Hernandez, Y.; Lotya, M.; Coleman, J. N.; Blau, W. J. *Adv. Mater.* **2009**, *21*, 2430.
- (15) Xu, Y. F.; Liu, Z. B.; Zhang, X. L.; Wang, Y.; Tian, J. G.; Huang, Y.; Ma, Y. F.; Zhang, X. Y.; Chen, Y. S. *Adv. Mater.* **2009**, *21*, 1275.

- (16) Zhou, Y.; Bao, Q. L.; Tang, L. A. L.; Zhong, Y. L.; Loh, K. P. *Chem. Mater.* **2009**, *21*, 2950.
- (17) Son, Y. W.; Cohen, M. L.; Louie, S. G. *Nature* **2006**, *444*, 347.
- (18) Barone, V.; Hod, O.; Scuseria, G. E. *Nano Lett.* **2006**, *6*, 2748.
- (19) Nomura, K.; MacDonald, A. H. *Phys. Rev. Lett.* **2006**, *96*, 256602.
- (20) Yang, L.; Cohen, M. L.; Louie, S. G. *Nano Lett.* **2007**, *7*, 3112.
- (21) Pedersen, T. G.; Flindt, C.; Pedersen, J.; Jauho, A. P.; Mortensen, N. A.; Pedersen, K. *Phys. Rev. B* **2008**, *77*, 245431.
- (22) Zhang, C.; Chen, L.; Ma, Z. S. *Phys. Rev. B* **2008**, *77*, 241402.
- (23) Li, X. L.; Wang, X. R.; Zhang, L.; Lee, S. W.; Dai, H. J. *Science* **2008**, *319*, 1229.
- (24) Han, M. Y.; Ozyilmaz, B.; Zhang, Y. B.; Kim, P. *Phys. Rev. Lett.* **2007**, *98*, 206805.
- (25) Dresselhaus, M. S.; Dresselhaus, G. *Adv. Phys.* **2002**, *51*, 1.
- (26) Schniepp, H. C.; Li, J. L.; McAllister, M. J.; Sai, H.; Herrera-Alonso, M.; Adamson, D. H.; Prud'homme, R. K.; Car, R.; Saville, D. A.; Aksay, I. A. *J. Phys. Chem. B* **2006**, *110*, 8535.
- (27) Qian, H. L.; Negri, F.; Wang, C. R.; Wang, Z. H. *J. Am. Chem. Soc.* **2008**, *130*, 17970.
- (28) Yang, X. Y.; Dou, X.; Rouhanipour, A.; Zhi, L. J.; Rader, H. J.; Mullen, K. *J. Am. Chem. Soc.* **2008**, *130*, 4216.
- (29) Yu, A. P.; Ramesh, P.; Itkis, M. E.; Bekyarova, E.; Haddon, R. C. *J. Phys. Chem. C* **2007**, *111*, 7565.
- (30) Wang, X. R.; Ouyang, Y. J.; Li, X. L.; Wang, H. L.; Guo, J.; Dai, H. J. *Phys. Rev. Lett.* **2008**, *100*, 206803.
- (31) Luo, Z. T.; Vora, P. M.; Mele, E. J.; Johnson, A. T. C.; Kikkawa, J. M. *Appl. Phys. Lett.* **2009**, *94*, 111909.
- (32) Frisch, M. J.; et al. *Gaussian 03*, revision E.01; Gaussian, Inc.: Wallingford, CT, 2004.
- (33) Wang, S. Q.; Gan, Q.; Zhang, Y. F.; Li, S. Y.; Xu, H. J.; Yang, G. Q. *ChemPhysChem* **2006**, *7*, 935.
- (34) Basche, T.; Kummer, S.; Brauchle, C. *Nature* **1995**, *373*, 132.
- (35) Tamarat, P.; Maali, A.; Lounis, B.; Orrit, M. *J. Phys. Chem. A* **2000**, *104*, 1.
- (36) Vincent, D. *Appl. Opt.* **2001**, *40*, 6646.
- (37) Tutt, L. W.; Kost, A. *Nature* **1992**, *356*, 225.
- (38) Joshi, M. P.; Mishra, S. R.; Rawat, H. S.; Mehendale, S. C.; Rustagi, K. C. *Appl. Phys. Lett.* **1993**, *62*, 1763.
- (39) Perry, J. W.; Mansour, K.; Lee, I. Y. S.; Wu, X. L.; Bedworth, P. V.; Chen, C. T.; Ng, D.; Marder, S. R.; Miles, P.; Wada, T.; Tian, M.; Sasabe, H. *Science* **1996**, *273*, 1533.
- (40) O'Flaherty, S. M.; Hold, S. V.; Cook, M. J.; Torres, T.; Chen, Y.; Hanack, M.; Blau, W. J. *Adv. Mater.* **2003**, *15*, 19.
- (41) Kost, A.; Tutt, L.; Klein, M. B.; Dougherty, T. K.; Elias, W. E. *Opt. Lett.* **1993**, *18*, 334.
- (42) Ozyilmaz, B.; Jarillo-Herrero, P.; Efetov, D.; Kim, P. *Appl. Phys. Lett.* **2007**, *91*, 192107.
- (43) Liu, G.; Zhuang, X. D.; Chen, Y.; Zhang, B.; Zhu, J. H.; Zhu, C. X.; Neoh, K. G.; Kang, E. T. *Appl. Phys. Lett.* **2009**, *95*, 253301.
- (44) Xia, F. N.; Farmer, D. B.; Lin, Y. M.; Avouris, P. *Nano Lett.* **2010**, *10*, 715.
- (45) Miller, D. A. B. *J. Opt. Soc. Am. B* **1984**, *1*, 857.
- (46) Elias, D. C.; Nair, R. R.; Mohiuddin, T. M. G.; Morozov, S. V.; Blake, P.; Halsall, M. P.; Ferrari, A. C.; Boukhalov, D. W.; Katsnelson, M. I.; Geim, A. K.; Novoselov, K. S. *Science* **2009**, *323*, 610.
- (47) Tommasini, M.; Castiglioni, C.; Zerbi, G. *Phys. Chem. Chem. Phys.* **2009**, *11*, 10185.
- (48) Prezzi, D.; Varsano, D.; Ruini, A.; Marini, A.; Molinari, E. *Phys. Rev. B* **2008**, *77*, 041404.
- (49) Castiglioni, C.; Negri, F.; Rigolio, M.; Zerbi, G. *J. Chem. Phys.* **2001**, *115*, 3769.
- (50) Ferrari, A. C.; Meyer, J. C.; Scardaci, V.; Casiraghi, C.; Lazzeri, M.; Mauri, F.; Piscanec, S.; Jiang, D.; Novoselov, K. S.; Roth, S.; Geim, A. K. *Phys. Rev. Lett.* **2006**, *97*, 187404.
- (51) Huang, M. Y.; Yan, H. G.; Chen, C. Y.; Song, D. H.; Heinz, T. F.; Hone, J. *Proc. Natl. Acad. Sci. U.S.A.* **2009**, *106*, 7304.
- (52) Dong, X. C.; Shi, Y. M.; Zhao, Y.; Chen, D. M.; Ye, J.; Yao, Y. G.; Gao, F.; Ni, Z. H.; Yu, T.; Shen, Z. X.; Huang, Y. X.; Chen, P.; Li, L. J. *Phys. Rev. Lett.* **2009**, *102*, 135501.
- (53) Malard, L. M.; Elias, D. C.; Alves, E. S.; Pimenta, M. A. *Phys. Rev. Lett.* **2008**, *101*, 257401.
- (54) Jung, N.; Kim, N.; Jockusch, S.; Turro, N. J.; Kim, P.; Brus, L. *Nano Lett.* **2009**, *9*, 4133.
- (55) Yang, L.; Park, C. H.; Son, Y. W.; Cohen, M. L.; Louie, S. G. *Phys. Rev. Lett.* **2007**, *99*, 186801.
- (56) Son, Y. W.; Cohen, M. L.; Louie, S. G. *Phys. Rev. Lett.* **2006**, *97*, 216803.
- (57) Zhen, Y. G.; Wang, C. R.; Wang, Z. H. *Chem. Commun.* **2010**, *46*, 1926.